WILEY-VCH

DOI:
Article type: Research News

Designer shape anisotropy on transistion metal dichalcogenide nanosheets

*Christian Martella, Carlo Mennucci, Alessio Lamperti, Emmanuele Cappelluti, Francesco Buatier de Mongeot and Alessandro Molle**

Dr. C. Martella, Dr. A. Lamperti, Dr. A. Molle
Laboratorio MDM, IMM-CNR, via C. Olivetti 2, I-20864, Agrate Brianza (MB), Italy
E-mail: christian.martella@mdm.imm.cnr.it, alessandro.molle@mdm.imm.cnr.it
Dr. C. Mennucci, Prof. F. Buatier de Mongeot
Dipartimento di Fisica, Università di Genova, via Dodecaneso 33, I-16146, Genova (Ge), Italy
Dr. C. Martella,
Istituto dei Sistemi Complessi (ISC)-CNR, U.O.S. Sapienza, 00185 Roma, Italy
Dr. E. Cappelluti,
Istituto di Struttura della Materia, Consiglio Nazionale delle Ricerche, I-34149 Trieste, Italy

MoS_2 and generally speaking, the wide family of transistion metal dichalcogenides represent a solid nanotechnology platform on which to engineer a wealth of new and outperforming applications involving two-dimensional (2D) materials. An even richer flexibility can be gained by extrinsically inducing an in-plane shape anisotropy of the nanosheets. Here we propose the synthesis of anisotropic MoS_2 nanosheets as a prototypical example in this respect starting from a highly conformal chemical vapor deposition on pre-patterend substrates and aiming at the more general purpose of tailoring anisotropy of 2D nanosheets by design. This is envisioned to be a suitable configuration for strain engineering as far as strain can be spatially redistributed in morphologically different regions. With a similar approach, both the optical and electronic properties of the 2D transition metal dichalcogenides can be tailored over macroscopic sample

areas in a self-organised fashion, thus paving the way for new applications in the field of optical metasurfaces, light harvesting and catalysis.

Main Text

1 – Transition metal dichalcogenides as nanotechnology platform

Transition metal dichalcogenides (TMDs) and their van der Waals (vdW) heterostructures constitute a class of two-dimensional (2D) layered materials offering an extraordinary potential for new nanotechnology applications and exploration of fundamental properties. [1–5]Among TMDs, MoS_2 has attracted an outstanding interest in its atomically thin form starting from the realization of a field effect transistor based on an ultimately thin MoS2 single-layer up to the integration in a logic chip. [6,7] Furthermore, the rich physics incorporated by MoS_2 and TMDs offers an unprecedented wealth of applications in nanoelectronics, optolectronics, nanophotonics and plasmonics, photovoltaics, catalysis, etc.[8–11]

An actual advantage of MoS_2/TMD based nanotechnology lies on the suitability to have them synthesized through relatively cost-effective massive production methods such as chemical exfoliation (CE) or chemical vapor deposition (CVD). While the CE approach can pave the way to a bio-compatible inkjet printing,[12] the use of CVD is more suited to yield scalability on a large area coverage and tunability of the morphological features down to the nanoscale, i.e. atomic thickness, conformality, etc. [13] Basically, most of the CVD methods for the synthesis of MoS_2 (TMD) nanosheets are settled in a controlled temperature tubular furnace ambient (see **Figure 1a**) where sulphur (i.e. the chalcogen) is evaporated from a powder solid state or supplied as precursor gas (e.g. H_2S and transferred through a non-reactive carrier gas (Ar, N_2, H_2) towards the high-temperature reaction with a metal-based precursor (e.g. Mo, MoO_x) eventually leading to a 2D crystal growth onto an inert substrate (eg. SiO_2, sapphire, etc.). Irrespectively to the specific chalcogen-rich precursor, 2D crystal growth results from vapor

phase reaction and precipitation of MoS_2 down to the substrate whenever a MoO_3 powder is used as metal precursor (vapor phase raction, VPR), or from the heterogeneous reaction at the surface of a Mo or MoO_x film previously grown on the substrate (sulfurization of a pre-deposited metal-based film, SPF), thus resulting in crystals with different size and structural quality (**Figure 1b)**.[14] High degree of crystallinity (microscaled grain, low structural disorder, well-defined crystal structure) is obtained in the VPR case (see the triangular crystals in the optical microscopy image in the bottom panel of **Figure 1c**) but with the disadvantage of a lower control of coverage, thickness uniformity, and of conformality. [15]These properties can be on the other hand highly improved by the SPF approach at the price of more pronounced granularity and texturing of the (polycrystalline) nanosheet (see the atomic force microscopy in **Figure 1c, top**). Growth promoters consisting of organic molecules, like perylene-3,4,9,10-tetracarboxylic acid tetrapotassium salt (PTAS), are also used to facilitate the uniform substrate-wetting so as to attain crystal grains with larger size.[16] The procedure can be easily extended to other chalcogenides in a carefully tailored parametric condition so as to give a quite universal guidance for the synthesis of a large number of individual TMDs or vdW heterostructures incorporating multiple TMD layers . [5]

Along with the atomic manipulation of TMDs synthesized via defect engineering or via layer pile-up in electronically coupled vdW heterostructures, shape manipulation of MoS_2 (TMDs) is an alternative route to tailor specific properties, and expand or amplify currently achievable properties in the as-deposited state by introducing an *extrinsic anisotropy*. [5,17]An extrinsic anisotropy can be imparted by forcing the morphology of a continuous flat nanosheet into an anisotropic corrugated shape without rupture. The so-induced shape anisotropy at the nano- or meso-scale represents an effective way to tune the chemical and physical properites of 2D TMD nanosheets, potentially leading to an expanded TMD nanotechnology platform which enables on-demand engineering of shape-sensitive properties. Thanks to the inherent tunability, this approach is comparatively advantageous over other intrinsically anisotropic 2D materials such

as black phosphorous,[18] tellurene,[19] and layered transition metal trichalcolgenides.[20] Furthermore, it is conceptually different from the intrinsic anisotropic features such as the armchair vs. zig-zag edge terminations or the in-plane vs. out-of-plane layer arrangement.

In this Research News, we envision a number of opportunities that can be inspired by the anisotropy design at the 2D level (taking MoS_2 as a case in point). The implication of the shape anisotropy in the strain engineering at the 2D level is discussed with focus on in-plane thermoelectric behavior and on the excitonic funnel effect. Finally, selected nanotechnology applications where to take an extra-benefit from the extrinsically induced shape anisotropy, are envisioned. These include the realization of optical metasurfaces, hybrid heterojunctions with mixed dimensionality, and a catalytic surface where to boost the hydrogen evolution reaction.

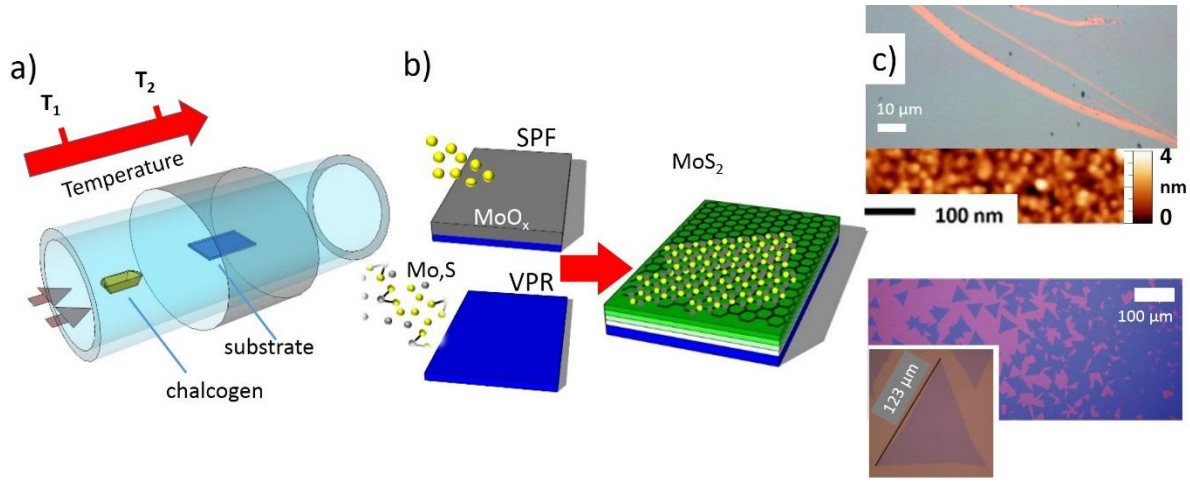

Figure 1 a) Pictorial sketch of the chemical vapour deposition (CVD) growth of transition metal dichalcogenides (TMDs) nanosheets. Chalcogen powder is heated above the evaporation temperature (T_1) in a quartz tube and a carrier gas (grey arrows) is used to transport vapours towards the hot ($T_2 > T_1$) central zone of a furnace where the metal precursor and substrate are placed. **b)** TMD growth occurs *via* heterogeneous solid-vapour reaction when the metal is in the form of a solid precursor film (SPF) or *via* homogeneous vapour phase reaction (VPR) when in the vapour phase. **c)** (Top) Optical microscope image showing the uniform growth of MoS_2 nanosheets obtained by means of the SPF-CVD approach. The pink lines are scratches intentionally made to expose the substrate. The atomic force microscope (AFM) topography of the MoS_2 nanosheets shows the nanoscale granular morphology Reproduced with permission.[14] (Bottom) Triangular domains of MoS_2 single crystals grown by means of the VPR-CVD approach. Adapted and reproduced with permission.[15]

2- Shape anisotropy in MoS_2 by design

Mechanically stretching a MoS_2 flake into a wrinkled sheet can be regarded as a prototypical method to induce shape anisotropy thus enabling the engineering of the electronic band-structure as a function of the local strain. [21] According to Martella et al. an alternative, bottom-up route to anisotropy shaping is based on the conformal, isomorphic growth of a MoS_2 nanosheet onto a nanopatterned substrate by leveraging the high degree of conformality gained from the SPF approach to the MoS_2 nanosheet growth (see **Figure 1b**). [22] Substrates in use are patterned in a self-organised fashion over large areas (cm^2) under the effect of ion beam projection lithography, a method which leads to the formation of a nanoscale ripple-pattern exploiting the interplay of erosive and diffusive effects as described by the Bradley-Harper model.[23,24] In detail, nanoscale one-directional rippled patterns are induced at the surface of a polycrystalline gold film, supported by an insulating/glass substrate, under irradiation with a high-flux defocused Ar ion beam at grazing incidence condition (82° off-normal) **Figure 2a.** At high ion doses the nanostructured polycrystalline Au film evolves into a perforated stencil mask which guides local etching of the SiO_2 substrate.

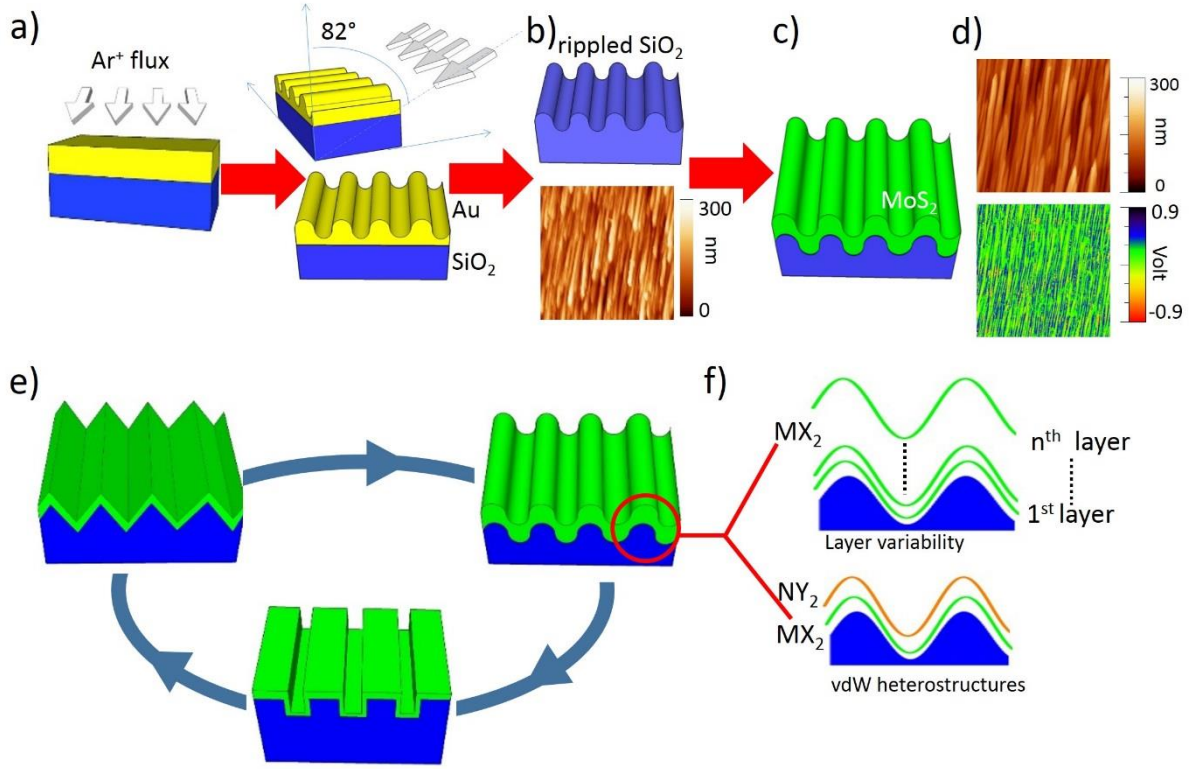

Figure 2 a) Process flow of the nano-patterning approach based on grazing incidence (82° off-normal) ion beam sputtering irradiation of a sacrificial gold mask deposited onto the SiO_2 substrate. **b**) Sketch (top) and AFM topography (bottom) of the nanoscale rippled pattern after the procedure described in panel a). **c)** Conformal SFP-CVD growth of the anisotropic MoS_2 nanosheets. **d)** Kelvin probe AFM investigation of the anisotropic MoS_2 nanosheets shown in c). Top and bottom panel compares topography and surface potential respectively. (a-d) Reprinted with permission. [22] Proposed strategies for the introduction of functional shape anisotropy into two-dimensional (2D) nanosheets by **e)** substrate pattern design and **f)** material design for a given pattern geometry.

Depending on the thickness of the Au stencil mask and on ion dose, the vertical height of the ripple pattern projected on a SiO_2 substrate can be tuned from tens to hundreds of nanometers. Following an SPF approach to MoS_2 growth, the nanopatterned SiO_2 substrate is covered with an MoO_x film (4 nm thick), and subsequently loaded into a hot wall furnace for the sulfurization resulting in continuous MoS_2 nanosheets down to the two layer limit (**Figure 2b**).[14,25] Morphological investigations based on atomic force microscopy (AFM) and transmission electron microscopy (TEM) reveal that the MoS_2 nanosheets grow conformally to the pre-patterned SiO_2 substrate thus mimicking the pristine anisotropic features, namely the local uniaxial curvature of the rippled profile and the periodic alternation of crests and valley in the scale of tens nanometers (**Figure 2c**). At the macroscopic scale, the rippled nanosheets show polarization dependent optical and vibrational properties, including an anisotropic angular distribution of the phonon mode scattering intensity with respect to the orientation of the ripple axis. The anisotropic character of the MoS_2 nanosheets is qualified both by a polarization-dependent Raman response and electronic workfunction variations at the local scale.[22] In detail, a red shift of the characteristic in-plane, E^1_{2g}, and of the out-of-plane, A_{1g}, Raman modes is detected in correspondence of the rippled valleys and an electronic surface potential modulation is observed in registry with the anisotropic rippled morphology (**Figure 2d**), both aspects being consistent with strain localization and charge doping at the nanoscale as consequence of the shape anisotropy, respectively.

This finding provides a preliminary guidance for tailoring the extrinsical shape anisotropy in 2D nanosheets. To this purpose, two different strategies are outlined in **Figure 2e** and **2f** based on the *geometry design* for a given 2D material, and on the *materials design* for a given geometry, respectively. In the former approach, the geometric profile is varied (**Figure 2e**) by means of conventional lithographic methods, in order to tailor the more appropriate shape according to the target application. Alternatively, the choice of the 2D material in use for a given pattern can provide an additional degree of freedom for designing the anisotropic system, therein comprising a variable number of chemically homogeneous layers (from MoS_2 single-layer to the multilayer, for instance) or the vertical stacking of different 2D materials in an anisotropic vdW heterostructure. The background concept is to expand the pristine properties of the 2D material by taking benefit from the added morphological anisotropy, as in the above-mentioned case of the corrugated MoS_2 nanosheet, so as to have a flexible and diversified portfolio of 2D materials addressing specific anisotropy features and/or functionalities. In this respect, obvious benefits can be obtained combining shape anisotropy and thickness-dependent electronic variability from a TMD single-layer to the multilayer or the symmetry-dependent valley polarization of the charge carriers that varies according to the odd or even number of stacked layers. [26–31] Furthermore, to an even wider degree of complexity and flexibility, vdW heterostructures offer a quite unlimited playground where to manipulate electronic and quasi-particle interactions and/or coupling. The two designer approaches are not mutually exclusive and they can be easily mixed up to expand the possible combinations and number of functionalities. In the following sections, attention will be more specifically paid to physical properties that are mostly affected by a shape anisotropy, and to the most promising applications in this regard.

3- Strain engineering

Given the wealth of the entangled degrees of freedom, a number of physical mechanisms can be exploited to functionalize the physical properties of anisotropically shaped TMDs (e.g. transport, optical, thermal, dielectric). Among them, one of the most interesting and investigated is the control by means of mechanical deformation, i.e. strain. At a uniform level, for instance, the possibility of tuning both the magnitude and character (e.g. direct vs. indirect) of the bandgap by means of homogeneous strain has been established. [32–37] Even at the local scale, strain tuning proved to be effective in modulating the band-gap. [21,38–47] The concept of a shape anisotropy may open a new path for the strain manipulation so as to achieve a close control of the local physical properties in registry with the morphological pattern. [47]

Here we discuss one of the most promising developments based on strain engineering of the bandgap with the aim of tailoring the transport and optical properties in anisotropic TMD nanosheets. [46,48] The schematics in **Figure 3a** illustrates a paradigm where anisotropic morphology and strain are mutually entangled. Such strain profile is reflected in an anisotropic modulation of the bandgap, which is expected to lead to anisotropic transport properties. In case of low-strain, we expect a different charge transport, parallel or perpendicular to the ridges.[49] In perspective, high strain rates (up to 10% in MoS2 or relatively lower in other TMDs) can eventually lead to a semiconductor-metal transition, which can be directionally oriented or spatially confined through a proper anisotropy design (see **Figure 3a**). [32,35–37,50,51] In the following, application to the excitonic funnel effects and in-plane thermoelectrics are envisaged as two outstanding perspectives in this respect.

Excitonic funnel effect. The strain-induced tuning of the band structure is at the base of the "excitonic funnel effect", namely a spatial localization or separation of the particle-hole excitations controlled by the bending of the valence/conduction band profile as a function of the applied local strain. In this scenario, the fascinating concept of a strain-engineered artificial

atom has been recently proposed, which consists of a nanoindented MoS_2 membrane where electron and hole charges are bound together in a radial geometry.[38,44] Due to the low electrostatic screening potential experienced by charges in TMDs in the form of a single or few layers, photoexcited electron-hole pairs usually interact via strong Coulomb attractions forming photoexcited quasiparticles (excitons) with a strong binding energy. Designer shape anisotropy as proposed in **Figure 2** and schemed in **Figure 3a** offers a framework where excitons can be forcedly confined into uniaxially oriented periodic regions and new outstanding effects can come into play.[21,52] Among the latter we can mention the funneling drift of excitons towards highly stressed crest regions where radiative recombination of excitons occurs followed by spatially localized photoluminescence (PL) emission, as reported for wrinkled MoS_2 flakes (see **Figure 3b** for an overview). [21]

As a perspective, anisotropic patterns based on a single-layer MoS_2 can give rise to the localization of differently bound particle-hole excitations according to the specific strength and real-space profile of the strain according to the diagram in **Figure 3c** (top). Conversely, charge separation can be possibly accessed by piling up additional MoS_2 layers in order to reduce dielectric screening, see **Figure 3c** (bottom). In this scenario, PL is a good probe to detect curvature-induced band bending which provokes funneling of excitons towards the top of the curved ridges where radiative recombination and photoluminescent emission takes place (see the schematics in **Figure 3b**).[21] The other way around, anisotropy design allows to tailor the curvature of the nanosheet surface profile in such a way that the corresponding wavelength of the PL emission can be selectively tuned. From this point of view, one could thus fabricate a nanoscale emitting grating in which spectrally tuned PL emission is spatially localised on the ripple crests.

Anisotropy-related in-plane thermoelectrics. Strain accumulation in TMD nanosheet is known to change the details of the electronic band structure and can be thus used to decouple the electrical conduction from the heat transport. This concept has been recently formulated for a

phosphorene nanosheet aiming at thermoelectric applications. [53] From this point of view, a tensile strain usually leads to a reduction in the thermal conductivity (see **Figure 3a** for the direction of high/low electrical and thermal conductivity), with a redshift in phonon peaks and positive Grüneisen parameter γ .[34] Furthermore, the power factor improves while the thermal conductivity remains low with respect to the bulk counterpart. In particular, monolayer MoS_2 has a $\gamma = 1.06$ and a thermal conductivity 2-3 orders of magnitude lower than graphene, prospecting a highly-performing thermoelectric material. [54–60] Introducing the figure of merit $ZT = 2S\sigma T/\kappa$, where S is the Seebeck coefficient, σ the electrical conductivity, κ the thermal conductivity of the material and T the absolute temperature, MoS_2 nanoribbons with different widths are predicted to reach ZT = 3.4 (p-type) , comparable to Si nanowires. [61] As shown in **Figure 3a,** a configuration in which the TMD nanosheets are anisotropically shaped allows to unbalance the electrical and thermal conductivity so as to maximize the ZT factor and thus lays the foundation of a prototypical in-plane thermoelectric functionality.

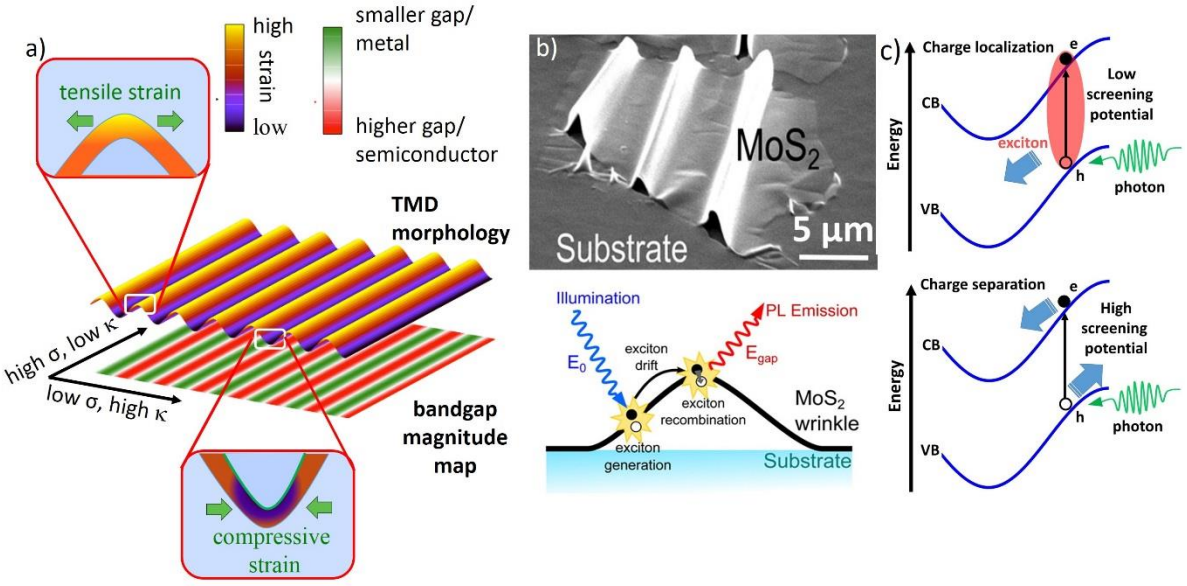

Figure 3 a) Strain intensity distribution in TMD nanosheets with anisotropic morphology. The model displays a representative configuration where tensile and compressive strain accumulates on the crests and on the valleys of the anisotropic profile respectively.Strain is expected to induce modification of the opto-electronic properties of the nanosheets at the local scale, thus resulting in a bandgap magnitude variability and the occurance of directions of high and low electrical (σ) and thermal (κ) conductivity, once the film is structured in anisotropic morphology. **b)** (Top) Scanning electron microscope image of strained rippled MoS_2 nanosheets obtained by deformation of an elastomeric substrate. (Bottom) Sketch of the exciton drift mechanism due to a funnel effect in strained MoS_2 nanosheets. Radiative recombination of excitons occurs at the crest of the MoS_2 wrinkles with a photoluminescence (PL) emission. Adapted and reprinted with permission. [21] **c)** Sketch of the generation of photo-excited electron-hole (e-h) pair between valence (VB) and conduction (CB) bands in strained MoS_2 nanosheets. Funnelling effect leads to exciton localization (top) or charge separation (bottom) depending on electronic-band bending and electrostatic screening potential.

4. Nanotechnology applications

Optical metasurfaces. In the previous section, shape anisotropy was meant as a tool for tuning the *local* electronic properties of the nanosheets by means of *local* strain engineering. Nevertheless, the anisotropic nanopatterned profiles proposed in **Figure 2** may be also used as platforms for the realization of optical *metasurfaces*. Optical metasurfaces are made of materials structured on the subwavelength scale in order to produce spatially varying optical constants which confer non-conventional effective optical properties in absorption, transmission and refraction measurements . [62–66] For instance, the metasurface model proposed by Arbabi et al., and depicted in **Figure 4a,** consists of a subwavelength-scale (meso or nano) array of amourphous silicon posts which act as an effective optical element. [63,66] The latter is capable of controlling the linear polarization of the incident light beam and to generate a circularly (or elliptically) polarized transmitted beam. On this ground, the conceptual picture in **Figure 4b** refers to a faceted periodic ripple template with a lateral periodicity well below the optical wavelength. The local shape anisotropy allows to couple light with the intrinsically different in-plane ($\varepsilon_{//}$) and an out-of-plane ($\varepsilon_{\perp}$) components of the dielectric tensor depending on impinging light polarization.[68] Analysis carried out by means of microellipsometry have already shown that the optical absorption of flat MoS_2 nanosheets is hindered when the electric field of t he incident light lies out of the plane of the TMDs nanosheets. [68] In particular,

this holds for the electromagnetic transition corresponding to exciton at wavelength, λ=450 nm (so called C-exciton). As a consequence, the metasurface of **Figure 4 b** naturally allows for a modulated absorption of light as a function of the light polarization. In particular, one could expect to selectively hinder optical absorption in correspondence of the long-lived C-exciton when the electric field polarization is perpendicular to the axis of the anisotropic structures, while conserving the conventional response of the flat TMD layer when light polarization is parallel to the ripple axis. [69]

In general, flat optics with designer metasurfaces allow even more complex wavefront shaping by leveraging the strong elastic interaction of light with nanostructured materials, conventionally chosen among noble metals or high index semiconductors and dielectrics due to their high refractive index [62][*All-dielectric metamaterials* S. Jahani and Z. Jacob Nature Nanotechnology **2016**, *11*, 23 DOI: 10.1038/NNANO.2015.304]. In this context, the exceptionally high refractive index of 2D TMDs, determines the accumulation of significant changes in amplitude and phase of the light wavefront, despite the reduced thickness of the TMD layer in the range of few monolayers ["Atomically thin optical lenses and gratings" J. Yang, Z. Wang, F.Wang, R.Xu, J. Tao, S. Zhang, Q. Qin, B. Luther-Davies, C. Jagadish, Z. Yu and Y. Lu *Light: Science & Applications* **2016,** *5,* e16046; doi:10.1038/lsa.2016.46]. For this reason the huge effective optical path lengths observed in TMDs are an order of magnitude larger than in thin metals (e.g Au) or graphene layers of comparable thickness. The textured TMDs templates, thus represent natural platforms for realizing atomically thin lenses or gratings. Given the strong interplay between electronic properties and optical effects in TMD nanosheets, including thickness-dependent bandgap variability, photoluminescence enhancement and exciton binding energy modification, [1,21,67] TMD-based optical metasurfaces with complex electro-optical functionality can be easily envisaged.

We also highlight the possibility to exploit the TMD metasurfaces as effective sources of non-linear optical generation owing to the break of the (out-of-plane) inversion symmetry selectively induced at the tilted facets of the nanosheets. [70] As a result, interaction with polarized light may lead to anisotropic generation or amplification of second (or higher) order harmonic electromagnetic field even when non-linear optical effects do not take place in the flat TMD geometry (e.g. for an even number of layers). [71–73]

Optical metasurface based on anisotropic TMD nanosheets (as in Figure 2) can also be functional for light harvesting in order to bring a substantial boost of the photo-current efficiencies reported for TMDs-based photovoltaic devices compared to the flat morphology. [74] Reflection losses at the nanosheets/air interface can be reduced over a broad spectral range due to an *index grading effect* which occurs when the interface is nanostructured with a sawtooth pattern profile endowed with a lateral periodicity and vertical amplitude respectively smaller (larger) than light wavelength.[75] Contrary to the abrupt change of refractive index occurring at a flat interface, a light beam experiences a smooth variation of the *effective* refractive index when propagating from the air to the patterned material. As a result, the reflectivity of the interface can be significantly reduced and the number of photons potentially absorbed by a photovoltaic device increases.

Hybrid heterostructures. A completely different approach to photon harvesting is to fabricate hybrid heterostructures with mixed dimensionalities where one- or zero-dimensional objects are interfaced with the anisotropic 2D surface.[76] In this context the 1-dimensional shape corrugation of the TMD template naturally lends itself to the formation of hybrid arrays of functional nanoparticles adopting a single step natural lithography. As an example, **Figure 4c** depicts a conceptual model where plasmonic metal nanowires are deposited on the sides of the anisotropic TMDs nanosheets by means of grazing incidence deposition**.** [77] Metal nanowires/nanoparticles, sustaining localized surface plasmon (LSP) resonances, will increase

the number of photons harvested by the TMDs via enhanced light scattering and/or near field amplification, **Figure 4d** (left). Both mechanisms stem from the coherent oscillation of the conduction electrons in the metal nanoparticles/nanowires at the plasmonic resonance. Plasmonic scatterers and nanoantennas (1D or 0D objects either located at the surface level or embedded) can thus be exploited to trap the light and increase the absorption probability into photovoltaic devices based on thin-film active layers.[78] Alternatively, one can exploit the non-radiative LSP decay channel which leads to the formation of energetic *hot electrons* in the metal; the latter in turn can be injected into the TMDs overcoming the (Schottky) potential barrier at the metal/semiconductor interface, thus increasing the overall photo-current in the photovoltaic device, **Figure 4d** (right). [79] By appropriately tailoring the plasmonic nanowire aspect ratio, one can easily redshift the LSP resonant wavelength towards the near-infrared (NIR) spectral range where, in general, the absorption cross section of TMDs is very weak, thus promoting sub-bandgap photon harvesting. [80,81]

Catalytic surfaces. A field where anisotropic TMD nanosheets may bring an additional value is the photo- or electrically induced water splitting. [82] We will focus here on the hydrogen evolution reaction (HER) as a paradigmatic example in this framework.[83] Due to the potential impact on the production of clean-energy, MoS_2 nanosheets have been also tested as catalytic material in water-splitting cells with the aim of replacing expensive metal catalysts with cost-effective solutions. At the cathode of the cell, the HER mechanism

$$2H^+ + 2e^- \rightarrow H_2$$

takes place through intermediate steps, which involve both adsorption and desorption of hydrogen. [10] The HER rate depends on the hydrogen binding energy of the catalytic material, ΔG_H, i.e. the difference between the adsorption and desorption free energy at the cathode. The optimal condition for HER catalytic material needs $\Delta G_H \sim 0$ eV in order to ensure that neither the adsorption nor the desorption step limits the overall reaction rate. In this respect, MoS_2 is promisingly benchmarked with other conventional metal catalysts according to the so called

"volcano" plot of the exchange current density vs. ΔG_H. [84] High catalytic activity was originally found in the electrically conductive 1T polymorph of MoS_2 where Mo has a octahedral coordination (**Figure 4e**, left). Conversely, the 2H MoS_2 polymorph, where Mo has a trigonal prismatic coordination (**Figure 4e**, left), is reported to have a catalytically inert basal plane and a high catalytic activity at the metallic edges where $\Delta G_H \sim 0$ is expected. [85] Therefore, one strategy to boost HER efficiency in MoS_2 and related TMDs is to increase the fraction of exposed active edges over the inert basal plane sites with *ad hoc* tailored and doped nanoparticles or nanostructures. Another strategy consists of strain or local phase engineering of the MoS_2 basal plane where a mixed 1T-2H atomic structure can be defined as shown in transmission electron microscopy image in **Figure 4e** (left). [86] In the former case, Li et al. showed that the creation of S-vacancies in the 2H phase lattice leads to strain field localization resulting in reduction of the hydrogen binding energy at these sites, **Figure 4e** (right). [87] In the latter case, Voiry et al. demonstrated that the local phase engineering via Li ion intercalation results in a reduced contact resistance between the basal plane and the cell electrode, thus increasing the number of charges injected into the catalyst and its electrical conductivity.[88]. Shape anisotropy engineering can boost the above-mentioned strategies in several ways. On one hand, the higher aspect ratio of the anisotropic MoS_2 nanosheets can increase the number of catalytically active sites by overbalancing the exposed edge at the grain boundaries. This aspect is advantageous also for other catalytic processes of relevance for MoS_2 such as the light-driven water disinfection: inactivation of organic pathogens proceeds via photo-generation of reactive oxygen species which are more effectively produced at edge sites .[82] Furthermore, the strain field associated with the anisotropic profile, **Figure 3**, can be exploited to tailor the light absorption bands for specific photo-induced catalytic reactions (e.g. phenol photooxidation) and/or to vary the electronic details of the catalytic activity (e.g. reduction of the hydrogen binding energy). On the other hand, the anisotropy-dependent tuning of the local charge distribution and electronic workfunction, **Figure 4f,** may represent an effective route to

minimize contact resistance between the basal plane and the electrodes thus making possible to outperform the catalytic activity of the flat geometry.

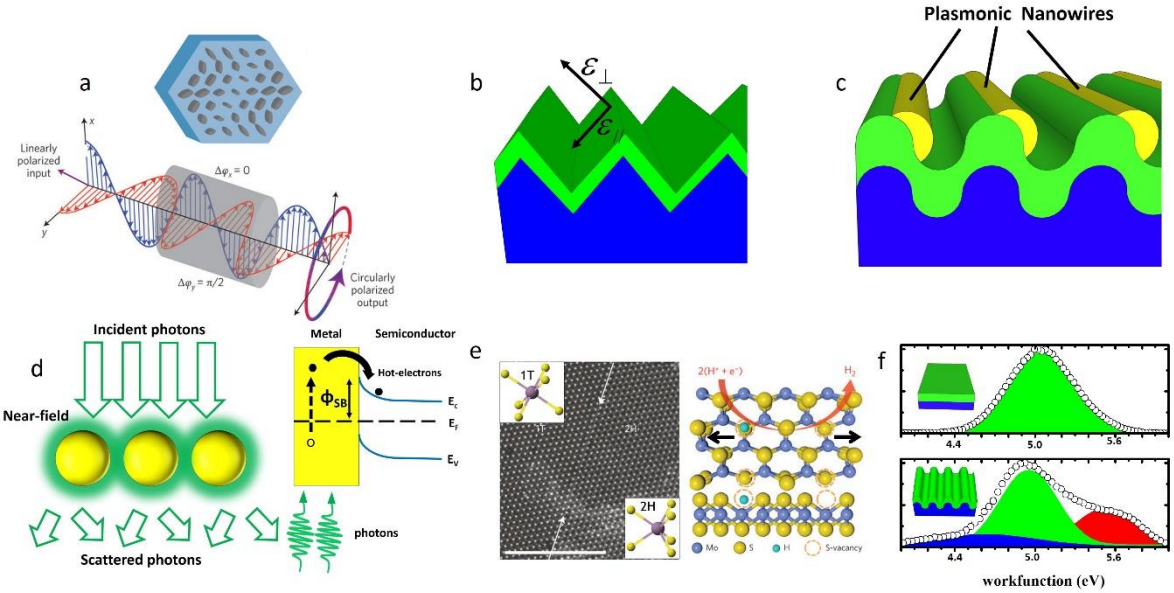

Figure 4 a) The optical metasurface consists of an array of subwavelength amourphous silicon posts and acts as an optical element able to transform the linear polarization of the incident light wavefront into a circular polarized transmitted wavefront. Adapted and reprinted with permission. [63] **b)** Conceptual model for an optical metasurface based on anisotropic TMD nanosheets. The different in-plane ($\varepsilon_{//}$) and an out-of-plane ($\varepsilon_{\perp}$) components of the dielectric tensor are expected to cause polarization-dependent optical absorption and non-linear optical effect. **c)** Conceptual model for a hybrid TMD/plasmonic heterostructure in view of photon harvesting in photovoltaic devices exploiting the effects depicted in the d) panel. **d)** (left) light scattering and near-field amplification or (right) injection of photon-generated *hot electrons* through the metal-semiconductor Schottky barrier (Φ_{SB}) formed at the mixed dimensional heteostructure. **e)** (left) High-resolution transmission electron microscope image of an atomically thin phase boundary (indicated by the arrows) between the 1T and 2H phases in a monolayered MoS2 nanosheet. Scale bar, 5 nm. Insets: Octahedral and trigonal prismatic coordination of the Mo atoms in the 1T and 2H phase of MoS_2, respectively. Adapted and reprinted with permission. [86] (Right) Model of the MoS_2 basal plane (top and lateral view) with sulphur vacancies leading to strain localization. The HER catalytic activity increases at the vacancy sites. Adapted and reprinted with permission. [87] **f)** Electronic-workfunction distribution in flat (top) and anisotropic MoS_2 nanosheets (bottom) grown by CVD. The modification of the electronic properties induced by the shape anisotropy is expected to play a significant role in improving the HER catalytic activity of the MoS_2 basal plane. Reprinted with permission.[22]

5- Perspectives and Outlook

Anisotropy design is here presented as a route for tuning locally the outstanding native properties of morphologically isotropic MoS_2 and related TMDs. In this Research News, we have spotlighted a methodology which enables to set them anisotropic on substrates of relevance in a broad range of applications. The resulting nanosheets look like a 2D rippled membrane where to devise new physical concepts or to enhance optical, plasmonic, and catalytic performances of the pristine materials. Strain engineering is taken as case in point as far as relevant properties such as the thermal/electronic transport or the exciton physics are drammatically affected by the anisotropy-dependent degreee of strain. On this background, anisotropic nanosheets are proposed as a platform where the optical response can be manipulated *ad hoc* forming optical metasurfaces, and where to host hybrid heterostructure for nanoplasmonics. Last but not least, anisotropic nanosheets are also envisaged as a model system to boost the catalytic performance of the hydrogen evolution reaction. We stress here that this list of representative examples aims at assessing the potential of anistropy design of MoS_2 and TMD nanosheets and highlights the potential of such platform for viable technology breakthroughs since material engineering at the 2D level is based on large-area maskless approaches

Acknowledgements
This research was partially funded by the MIUR under the PRIN 2015 Grant No. 2015WTW7J3. C. Mennucci and F. Buatier de Mongeot acknowledge financial support from the Compagnia di San Paolo in the framework of Project ID ROL 9361 and of the MAECI in the framework of the Italy–Egypt bilateral protocol. E. Cappelluti acknowledges financial support from the European project FP7-PEOPLE-2013-CIG "LSIE 2D". A. Molle acknowledges financial support from the Fondazione CARIPLO and Regione Lombardia for the project "Crystel" (ref. no. 2016-0978). C. Martella, A. Lamperti, and A. Molle acknowledge Regione Lombardia

(Accordo Quadro Regione Lombardia-CNR, project: "I-ZEB Verso Edifici Intelligenti a Energia Zero per la crescita della città intelligente") for financial support. All authors had given approval to the final version of the manuscript.

Received: ((will be filled in by the editorial staff))
Revised: ((will be filled in by the editorial staff))
Published online: ((will be filled in by the editorial staff))

References

[1] M. Chhowalla, H. S. Shin, G. Eda, L.-J. Li, K. P. Loh, H. Zhang, *Nat. Chem.* **2013**, *5*, 263.
[2] I. S. Kim, V. K. Sangwan, D. Jariwala, J. D. Wood, S. Park, K.-S. Chen, F. Shi, F. Ruiz-Zepeda, A. Ponce, M. Jose-Yacaman, V. P. Dravid, T. J. Marks, M. C. Hersam, L. J. Lauhon, *ACS Nano* **2014**, *8*, 10551.
[3] C. Tan, Z. Lai, H. Zhang, *Adv. Mater.* **2017**, 1701392.
[4] B. Dubertret, T. Heine, M. Terrones, *Acc. Chem. Res.* **2015**, *48*, 1.
[5] K. S. Novoselov, A. Mishchenko, A. Carvalho, A. H. Castro Neto, *Science* **2016**, *353*, aac9439.
[6] B. Radisavljevic, A. Radenovic, J. Brivio, V. Giacometti, A. Kis, *Nat. Nanotechnol.* **2011**, *6*, 147.
[7] S. Wachter, D. K. Polyushkin, O. Bethge, T. Mueller, *Nat. Commun.* **2017**, *8*, 14948.
[8] G. Fiori, F. Bonaccorso, G. Iannaccone, T. Palacios, D. Neumaier, A. Seabaugh, S. K. Banerjee, L. Colombo, *Nat. Nanotechnol.* **2014**, *9*, 768.
[9] F. H. L. Koppens, T. Mueller, P. Avouris, A. C. Ferrari, M. S. Vitiello, M. Polini, *Nat. Nanotechnol.* **2014**, *9*, 780.
[10] J. D. Benck, T. R. Hellstern, J. Kibsgaard, P. Chakthranont, T. F. Jaramillo, *ACS Catal.* **2014**, *4*, 3957.
[11] G. Eda, S. A. Maier, *ACS Nano* **2013**, *7*, 5660.
[12] D. McManus, S. Vranic, F. Withers, V. Sanchez-Romaguera, M. Macucci, H. Yang, R. Sorrentino, K. Parvez, S.-K. Son, G. Iannaccone, K. Kostarelos, G. Fiori, C. Casiraghi, *Nat. Nanotechnol.* **2017**, *12*, 343.
[13] Y. Shi, H. Li, L.-J. Li, *Chem. Soc. Rev.* **2015**, *44*, 2744.
[14] S. Vangelista, E. Cinquanta, C. Martella, M. Alia, M. Longo, A. Lamperti, R. Mantovan, F. B. Basset, F. Pezzoli, A. Molle, *Nanotechnology* **2016**, *27*, 175703.
[15] A. M. van der Zande, P. Y. Huang, D. A. Chenet, T. C. Berkelbach, Y. You, G.-H. Lee, T. F. Heinz, D. R. Reichman, D. A. Muller, J. C. Hone, *Nat. Mater.* **2013**, *12*, 554.
[16] X. Ling, Y.-H. Lee, Y. Lin, W. Fang, L. Yu, M. S. Dresselhaus, J. Kong, *Nano Lett.* **2014**, *14*, 464.
[17] Z. Lin, B. R. Carvalho, E. Kahn, R. Lv, R. Rao, H. Terrones, M. A. Pimenta, M. Terrones, *2D Mater.* **2016**, *3*, 22002.
[18] F. Xia, H. Wang, Y. Jia, *Nat. Commun.* **2014**, *5*, 666.

[19] Y. Du, G. Qiu, Y. Wang, M. Si, X. Xu, W. Wu, P. D. Ye, *Nano Lett.* **2017**, *17*, 3965.
[20] Y. Jin, X. Li, J. Yang, *Phys. Chem. Chem. Phys.* **2015**, *17*, 18665.
[21] A. Castellanos-Gomez, R. Roldán, E. Cappelluti, M. Buscema, F. Guinea, H. S. J. van der Zant, G. A. Steele, *Nano Lett.* **2013**, *13*, 5361.
[22] C. Martella, C. Mennucci, E. Cinquanta, A. Lamperti, E. Cappelluti, F. Buatier de Mongeot, A. Molle, *Adv. Mater.* **2017**, *29*, 1605785.
[23] A. Toma, D. Chiappe, B. Šetina Batič, M. Godec, M. Jenko, F. Buatier de Mongeot, *Phys. Rev. B* **2008**, *78*, 153406.
[24] R. M. Bradley, J. M. E. Harper, *J. Vac. Sci. Technol. A Vacuum, Surfaces, Film.* **1988**, *6*, 2390.
[25] C. Martella, P. Melloni, E. Cinquanta, E. Cianci, M. Alia, M. Longo, A. Lamperti, S. Vangelista, M. Fanciulli, A. Molle, *Adv. Electron. Mater.* **2016**, *2*, 1600330.
[26] K. F. Mak, C. Lee, J. Hone, J. Shan, T. F. Heinz, *Phys. Rev. Lett.* **2010**, *105*, 136805.
[27] C. Lee, H. Yan, L. E. Brus, T. F. Heinz, J. Hone, S. Ryu, *ACS Nano* **2010**, *4*, 2695.
[28] Y. Yu, Y. Yu, Y. Cai, W. Li, A. Gurarslan, H. Peelaers, D. E. Aspnes, C. G. Van de Walle, N. V. Nguyen, Y.-W. Zhang, L. Cao, *Sci. Rep.* **2015**, *5*, 16996.
[29] H. Zeng, J. Dai, W. Yao, D. Xiao, X. Cui, *Nat. Nanotechnol.* **2012**, *7*, 490.
[30] S. Wu, J. S. Ross, G.-B. Liu, G. Aivazian, A. Jones, Z. Fei, W. Zhu, D. Xiao, W. Yao, D. Cobden, X. Xu, *Nat. Phys.* **2013**, *9*, 149.
[31] K. F. Mak, K. He, J. Shan, T. F. Heinz, *Nat. Nanotechnol.* **2012**, *7*, 494.
[32] P. Johari, V. B. Shenoy, *ACS Nano* **2012**, *6*, 5449.
[33] H. Peelaers, C. G. Van de Walle, *Phys. Rev. B* **2012**, *86*, 241401.
[34] H. J. Conley, B. Wang, J. I. Ziegler, R. F. Haglund, S. T. Pantelides, K. I. Bolotin, *Nano Lett.* **2013**, *13*, 3626.
[35] E. Scalise, M. Houssa, G. Pourtois, V. Afanas'ev, A. Stesmans, *Nano Res.* **2012**, *5*, 43.
[36] W. S. Yun, S. W. Han, S. C. Hong, I. G. Kim, J. D. Lee, *Phys. Rev. B* **2012**, *85*, 33305.
[37] S. Bhattacharyya, T. Pandey, A. K. Singh, *Nanotechnology* **2014**, *25*, 465701.
[38] J. Feng, X. Qian, C.-W. Huang, J. Li, *Nat. Photonics* **2012**, *6*, 866.
[39] A. Michail, N. Delikoukos, J. Parthenios, C. Galiotis, K. Papagelis, *Appl. Phys. Lett.* **2016**, *108*, 173102.
[40] J. Krustok, T. Raadik, R. Jaaniso, V. Kiisk, I. Sildos, M. Marandi, H.-P. Komsa, B. Li, X. Zhang, Y. Gong, P. M. Ajayan, *Appl. Phys. Lett.* **2016**, *109*, 253106.
[41] S. Kumar, A. Kaczmarczyk, B. D. Gerardot, *Nano Lett.* **2015**, *15*, 7567.
[42] K.-D. Park, O. Khatib, V. Kravtsov, G. Clark, X. Xu, M. B. Raschke, *Nano Lett.* **2016**, *16*, 2621.
[43] S. Luo, G. Hao, Y. Fan, L. Kou, C. He, X. Qi, C. Tang, J. Li, K. Huang, J. Zhong, *Nanotechnology* **2015**, *26*, 105705.
[44] H. Li, A. W. Contryman, X. Qian, S. M. Ardakani, Y. Gong, X. Wang, J. M. Weisse, C. H. Lee, J. Zhao, P. M. Ajayan, J. Li, H. C. Manoharan, X. Zheng, *Nat. Commun.* **2015**, *6*, 7381.
[45] B. G. Shin, G. H. Han, S. J. Yun, H. M. Oh, J. J. Bae, Y. J. Song, C.-Y. Park, Y. H. Lee, *Adv. Mater.* **2016**, *28*, 9378.
[46] R. Roldán, A. Castellanos-Gomez, E. Cappelluti, F. Guinea, *J. Phys. Condens. Matter* **2015**, *27*, 313201.
[47] S.-W. Wang, H. Medina, K.-B. Hong, C.-C. Wu, Y. Qu, A. Manikandan, T.-Y. Su, P.-T. Lee, Z.-Q. Huang, Z. Wang, F.-C. Chuang, H.-C. Kuo, Y.-L. Chueh, *ACS Nano* **2017**, acsnano.7b02444.
[48] J. Quereda, P. San-Jose, V. Parente, L. Vaquero-Garzon, A. J. Molina-Mendoza, N. Agraït, G. Rubio-Bollinger, F. Guinea, R. Roldán, A. Castellanos-Gomez, *Nano Lett.* **2016**, *16*, 2931.
[49] T. Shen, A. V. Penumatcha, J. Appenzeller, *ACS Nano* **2016**, *10*, 4712.

[50] M. Ghorbani-Asl, S. Borini, A. Kuc, T. Heine, *Phys. Rev. B* **2013**, *87*, 235434.
[51] S. Song, D. H. Keum, S. Cho, D. Perello, Y. Kim, Y. H. Lee, *Nano Lett.* **2016**, *16*, 188.
[52] P. San-Jose, V. Parente, F. Guinea, R. Roldán, E. Prada, *Phys. Rev. X* **2016**, *6*, 31046.
[53] R. Fei, A. Faghaninia, R. Soklaski, J.-A. Yan, C. Lo, L. Yang, *Nano Lett.* **2014**, *14*, 6393.
[54] Y. Cai, J. Lan, G. Zhang, Y.-W. Zhang, *Phys. Rev. B* **2014**, *89*, 35438.
[55] X. Liu, G. Zhang, Q.-X. Pei, Y.-W. Zhang, *Appl. Phys. Lett.* **2013**, *103*, 133113.
[56] W. Li, J. Carrete, N. Mingo, *Appl. Phys. Lett.* **2013**, *103*, 253103.
[57] J.-W. Jiang, H. S. Park, T. Rabczuk, *J. Appl. Phys.* **2013**, *114*, 64307.
[58] X. Wei, Y. Wang, Y. Shen, G. Xie, H. Xiao, J. Zhong, G. Zhang, *Appl. Phys. Lett.* **2014**, *105*, 103902.
[59] S. Sahoo, A. P. S. Gaur, M. Ahmadi, M. J.-F. Guinel, R. S. Katiyar, *J. Phys. Chem. C* **2013**, *117*, 9042.
[60] R. Yan, J. R. Simpson, S. Bertolazzi, J. Brivio, M. Watson, X. Wu, A. Kis, T. Luo, A. R. Hight Walker, H. G. Xing, *ACS Nano* **2014**, *8*, 986.
[61] D. D. Fan, H. J. Liu, L. Cheng, P. H. Jiang, J. Shi, X. F. Tang, *Appl. Phys. Lett.* **2014**, *105*, 133113.
[62] N. Yu, F. Capasso, *Nat. Mater.* **2014**, *13*, 139.
[63] R. Zia, *Nat. Nanotechnol.* **2015**, *10*, 913.
[64] F. Aieta, P. Genevet, M. A. Kats, N. Yu, R. Blanchard, Z. Gaburro, F. Capasso, *Nano Lett.* **2012**, *12*, 4932.
[65] I. Dolev, I. Epstein, A. Arie, *Phys. Rev. Lett.* **2012**, *109*, 203903.
[66] A. Arbabi, Y. Horie, M. Bagheri, A. Faraon, *Nat. Nanotechnol.* **2015**, *10*, 937.
[67] H.-P. Komsa, A. V. Krasheninnikov, *Phys. Rev. B* **2012**, *86*, 241201.
[68] U. Wurstbauer, B. Miller, E. Parzinger, A. W. Holleitner, *J. Phys. D. Appl. Phys.* **2017**, *50*, 173001.
[69] L. Wang, Z. Wang, H.-Y. Wang, G. Grinblat, Y.-L. Huang, D. Wang, X.-H. Ye, X.-B. Li, Q. Bao, A.-S. Wee, S. A. Maier, Q.-D. Chen, M.-L. Zhong, C.-W. Qiu, H.-B. Sun, *Nat. Commun.* **2017**, *8*, 13906.
[70] X. Yin, Z. Ye, D. A. Chenet, Y. Ye, K. O'Brien, J. C. Hone, X. Zhang, *Science* **2014**, *344*, 488.
[71] H. R. Gutiérrez, N. Perea-López, A. L. Elías, A. Berkdemir, B. Wang, R. Lv, F. López-Urías, V. H. Crespi, H. Terrones, M. Terrones, *Nano Lett.* **2013**, *13*, 3447.
[72] A. Belardini, M. C. Larciprete, M. Centini, E. Fazio, C. Sibilia, M. Bertolotti, A. Toma, D. Chiappe, F. Buatier de Mongeot, *Opt. Express* **2009**, *17*, 3603.
[73] Y. Li, Y. Rao, K. F. Mak, Y. You, S. Wang, C. R. Dean, T. F. Heinz, *Nano Lett.* **2013**, *13*, 3329.
[74] L. Britnell, R. M. Ribeiro, A. Eckmann, R. Jalil, B. D. Belle, A. Mishchenko, Y.-J. Kim, R. V Gorbachev, T. Georgiou, S. V Morozov, A. N. Grigorenko, A. K. Geim, C. Casiraghi, A. H. Castro Neto, K. S. Novoselov, *Science* **2013**, *340*, 1311.
[75] P. Vukusic, J. R. Sambles, *Nature* **2003**, *424*, 852.
[76] D. Jariwala, T. J. Marks, M. C. Hersam, *Nat. Mater.* **2016**, *16*, 170.
[77] A. Toma, D. Chiappe, D. Massabò, C. Boragno, F. Buatier de Mongeot, *Appl. Phys. Lett.* **2008**, *93*, 163104.
[78] H. A. Atwater, A. Polman, *Nat. Mater.* **2010**, *9*, 205.
[79] M. W. Knight, H. Sobhani, P. Nordlander, N. J. Halas, *Science* **2011**, *332*, 702.
[80] M. C. Giordano, D. Repetto, C. Mennucci, A. Carrara, F. B. de Mongeot, *Nanotechnology* **2016**, *27*, 495201.
[81] G. Della Valle, D. Polli, P. Biagioni, C. Martella, M. C. Giordano, M. Finazzi, S. Longhi, L. Duò, G. Cerullo, F. Buatier de Mongeot, *Phys. Rev. B* **2015**, *91*, 235440.
[82] C. Liu, D. Kong, P.-C. Hsu, H. Yuan, H.-W. Lee, Y. Liu, H. Wang, S. Wang, K. Yan,

D. Lin, P. A. Maraccini, K. M. Parker, A. B. Boehm, Y. Cui, *Nat. Nanotechnol.* **2016**, *11*, 1098.
[83] D. Voiry, M. Salehi, R. Silva, T. Fujita, M. Chen, T. Asefa, V. B. Shenoy, G. Eda, M. Chhowalla, *Nano Lett.* **2013**, *13*, 6222.
[84] T. F. Jaramillo, K. P. Jørgensen, J. Bonde, J. H. Nielsen, S. Horch, I. Chorkendorff, *Science* **2007**, *317*, 100.
[85] J. Kibsgaard, Z. Chen, B. N. Reinecke, T. F. Jaramillo, *Nat. Mater.* **2012**, *11*, 963.
[86] R. Kappera, D. Voiry, S. E. Yalcin, B. Branch, G. Gupta, A. D. Mohite, M. Chhowalla, *Nat. Mater.* **2014**, *13*, 1128.
[87] H. Li, C. Tsai, A. L. Koh, L. Cai, A. W. Contryman, A. H. Fragapane, J. Zhao, H. S. Han, H. C. Manoharan, F. Abild-Pedersen, J. K. Nørskov, X. Zheng, *Nat. Mater.* **2015**, *15*, 48.
[88] D. Voiry, R. Fullon, J. Yang, C. de Carvalho Castro e Silva, R. Kappera, I. Bozkurt, D. Kaplan, M. J. Lagos, P. E. Batson, G. Gupta, A. D. Mohite, L. Dong, D. Er, V. B. Shenoy, T. Asefa, M. Chhowalla, *Nat. Mater.* **2016**, *15*, 1003.